UDK 661.846:52-334.2
Original scientific article/Izvirni znanstveni članek

ISSN 1580-2949
Mater. Tehnol.

EFFECT OF Y ON THE MECHANICAL PROPERTIES AND CORROSION RESISTANCE OF AS-EXTRUDED Mg-4Sn ALLOYS

VPLIV Y NA MEHANSKE LASTNOSTI IN KOROZIJSKO ODPORNOST EKSTRUDIRANIH Mg-4Sn ZLITIN

Qiuli Chen[1], Zheng Jia[1,2*], Xiaowei Niu[2], Ayong Hu[1], Feida Ji[1], Chongrui Liu[1], Qianhe Cui[1], Yongzhi Yu[1]

[1]College of Mechanical Engineering, Shenyang University, Shenyang 110044
[2]College of Environment, Liaoning Province Environmental Pollution Remediation Professional Technology Innovation Center & Shenyang Key Laboratory of Collaborative Technology Innovation for Industrial Pollution Reduction and Carbon Reduction, Shenyang University, Shenyang 110044, China

Prejem rokopisa – received: 2024-07-23; sprejem za objavo – accepted for publication: 2024-10-10

doi:10.17222/mit.2024.1259

In this study, the effects of Y element on the microstructure, mechanical properties and corrosion resistance of an extruded T4 alloy at room temperature were studied by comparing the as-extruded Mg-4Sn (T4) and Mg-4Sn-1Y (TW41) alloys. The results showed that the second phase of the as-extruded T4 alloy is mainly the Mg_2Sn phase, while the ternary MgSnY and Mg_2Sn phases mainly precipitate after the addition of Y element. Incomplete dynamic recrystallization of the two alloys occurs during the extrusion process, and the addition of Y element can promote dynamic recrystallization and refinement of the grains in T4 alloy. At room temperature, TW41 alloy has higher strength compared to T4 alloy, with tensile and yield strengths of 228 MPa and 165 MPa, respectively, but the elongation and corrosion resistance are reduced. Grain refinement is believed to play the key role in improving the yield strength of TW41 alloy, while the deterioration of the corrosion resistance of TW41 alloy is mainly attributed to the increase in the grain boundary density caused by grain refinement, accelerating the dissolution of the alloy anode.

Key words: Mg-Sn alloy, alloying, mechanical properties, corrosive properties

V članku avtorji opisujejo vpliv dodatka itrija (Y) na mikrostrukturo, mehanske lastnosti in odpornost proti koroziji zlitin na osnovi Mg in Si. Med seboj so pri sobni temperaturi primerjali ekstrudirani zlitini tipa Mg-4Sn (T4) in Mg-4Sn-1Y (TW41). Rezultati raziskave so pokazali, da v prvi ekstrudirani zlitini kot sekundarna faza nastopa Mg_2Sn. V zlitini z dodatkom Y pa nastopata kot sekundarni fazi tako Mg_2Sn kot tudi MgSnY. Med procesom ekstruzije je pri obeh zlitinah prišlo do nepopolne dinamične rekristalizacije. Vendar je dodatek Y pospešil dinamično rekristalizacijo in udrobljenje (zmanjšanje velikosti kristalnih zrn) v zlitini TW41. Pri sobni temperaturi ima ta zlitina višjo natezno trdnost (228 MPa) in mejo plastičnosti (165 MPa) kot zlitina T4, znižali pa sta se vrednosti za raztezek in odpornost proti koroziji. Zmanjšanje velikosti zrn v zlitini TW41 je povzročilo izboljšanje meje plastičnosti. Poslabšanje odpornosti proti koroziji pa je posledica povečanja števila oz. gostote kristalnih mej, kar pospešuje anodno raztapljanje zlitine.

Ključne besede: Mg-Sn zlitine, legiranje, mehanske in korozijske lastnosti

1 INTRODUCTION

Magnesium alloy is a lightweight metal alloy that has attracted attention for its excellent machinability. Compared to other commonly used metal alloys, magnesium alloys have a lower density, higher specific strength, and higher specific stiffness, making them ideal for applications that require efficient fuel and weight reduction, such as aerospace and automotive manufacturing.[1–3] In these high-performance applications, the mechanical properties and corrosion resistance of the material are critical. Among them, improving the mechanical properties of magnesium alloys is the basic requirement for the wide application of magnesium alloys, and the mechanical properties of magnesium alloys can usually be improved by adding alloying elements to them to optimize the alloy composition and plastic deformation.[4–6] For example, Sadeddin et al.[7] studied the effects of different Zr additions (0, 0.5 and 1) *w*/% and extrusion ratios (6:1 and 12:1) on the microstructure and mechanical properties of Mg-5Sn alloys, and found that an addition of Zr could significantly refine the microstructure of the alloy so that the microstructure of the as-cast alloy gradually changed from dendritic to nearly spherical. Moreover, the addition of Zr can promote the precipitation of Mg_2Sn phase and improve the thermal stability of the alloy during high-temperature homogenization. In addition, the grains of the alloy are significantly refined after hot extrusion deformation, and the dynamic recrystallization and twinning generated during the extrusion process can effectively improve the mechanical properties of Mg-5Sn-xZr alloy.

On the other hand, many studies have found that magnesium is chemically active and susceptible to oxidation and corrosion, which can lead to degradation of material properties and impairment of structural integrity.[8–10] Therefore, corrosion resistance improvement and protection of magnesium alloys is the focus of research

*Corresponding author's e-mail:
jz140@163.com (Zheng Jia)

to further broaden their applications. Some studies have shown that methods such as surface coating and alloying have been used to improve the corrosion resistance of magnesium alloys so that they meet the needs of different applications.[11,12] For example, Ha et al.[13] studied the corrosion behavior of an as-extruded Mg-5Sn-(1–4 *w*/%) Zn alloy in a 0.6 M NaCl solution using the hydrogen precipitation weight loss test and electrochemical test. They found that the addition of a small amount of Zn can improve the corrosion resistance of Mg-5Sn alloy, while the addition of too much Zn will rather reduce the corrosion resistance of the alloy, where Mg-5Sn-2Zn has the lowest corrosion rate and the best corrosion resistance.

Therefore, alloying and plastic deformation are comprehensive and optimized means for improving the mechanical properties and corrosion resistance of magnesium alloys, which is crucial for ensuring their long-lasting durability in demanding engineering applications. In order to develop new magnesium alloys, the role of different alloying elements on magnesium alloys should be considered comprehensively. At present, Mg-Sn alloys have become a hot spot in the field of magnesium alloy research, which is due to the significant precipitation strengthening effect of the Sn element in Mg alloys. Moreover, the Mg_2Sn phase precipitated in Mg-Sn alloys has a high hardness, a high melting point, and good thermal stability, which can effectively improve the mechanical properties of magnesium alloys.[14] In addition, Sn can also improve the corrosion resistance of magnesium and its alloys, but the mechanical properties and corrosion resistance of Mg-Sn binary alloys at room temperature are still not ideal due to the existence of Mg_2Sn phases distributed in the network along the grain boundaries. Yang et al.[15] reported that an addition of the Y element to Mg-0.5Sn would refine the grains of the extruded alloy and significantly improve the mechanical properties of the alloy, with the ultimate tensile strength and elongation increasing by 21 % and 191 %, respectively. At the same time, the addition of the Y element forms the Sn_3Y_5 phase and inhibits the precipitation of the Mg_2Sn phase. It has been reported that rare earth elements can occupy the pores of the oxide film that forms on the surfaces of rare earths, thus preventing the diffusion of metal atoms.[16] Yu et al.[17] found that the protective properties of the oxide film formed due to the addition of Y element to the Mg-Sn alloy can be improved, providing good protection for the matrix and preventing further oxidation of the matrix. In addition, the oxide film of Mg-Sn-Y has good adhesion to the substrate, thus improving the corrosion resistance of the alloy.

In summary, the rare earth element Y can change the type of the second phase in an alloy and realize the refinement of the alloy microstructure, thereby improving the mechanical properties and corrosion resistance of the alloy. In view of this, in order to introduce Mg-Sn-based alloys into more fields, based on Mg-4Sn alloys, our alloys were prepared using homogenization heat treatment and back extrusion. The effects of a 1 *w*/% Y addition on the mechanical properties and corrosion resistance of extruded Mg-4Sn alloys were systematically studied to improve the comprehensive properties of Mg-Sn-based alloys.

2 EXPERIMENTAL METHODS

In this experiment, the as-cast Mg-4Sn (T4) and Mg-4Sn-1Y (TW41) alloys were prepared in pit resistance furnaces (RJ2 series, Hankou Electric Furnace Company, Wuhan, China) using industrially pure Mg (99.9 *w*/%), pure Sn (99.9 *w*/%) and Mg-25%Y master alloys as the raw materials. The melting process was as follows: firstly, pure magnesium was placed in a preheated crucible and heated to 730 °C. After pure magnesium was completely melted, the alloying element Sn was added and stirred in thoroughly. After that, the melt temperature was raised to 760 °C and the master alloy Mg-25%Y was added. After the alloy was completely melted, it was thoroughly stirred and cooled to 720 °C for 30 min. The melt was then poured into a mold with a diameter of 65 mm and a height of 240 mm under the protection of a mixed gas (CO_2:SF_6=2:1) for natural cooling and molding. In order to reduce or eliminate the intragranular segregation of the alloy, the cast alloy was homogenized at a temperature of 400 °C for 24 h in a box-type resistance furnace (1400 °C manual door box-type furnace) and cooled by water quenching. The obtained homogenized alloy was reverse extruded using a hydraulic press (600-ton vertical hydraulic press) at an extrusion temperature of 300 °C and an extrusion speed of 1 mm/s to obtain a bar with a diameter of 12 mm (an extrusion ratio of 14:1). The actual composition of the alloy was measured by an inductively coupled plasma spectrometer (Plasma 2000), and the results are shown in **Table 1**. The phase morphology was observed by a S4800 scanning electron microscope (SEM) (Hitachi S-4800), and the elemental composition of the phase was detected with the included energy dispersive spectrometer (EDS). Electron backscatter diffraction (EBSD) was used to obtain grain orientation information from the samples, and the data were analyzed by Channel 5 software.

The tensile mechanical properties of the extruded alloy at room temperature were tested with a Shimadzu AG-X (100 kN) electronic universal tensile testing machine. The sampling standard was in accordance with the national standard (GB/T 228.1-2021), and the tensile speed was 1 mm/min. The polarization curve and impedance spectrum were measured with a three-electrode electrochemical workstation (CHI660E) in a 3.5 *w*/% NaCl solution, in which the saturated calomel electrode was the reference electrode (RE), the platinum electrode was the auxiliary electrode (CE), and the working electrode (WE) was the sample to be tested. The hydrogen evolution-weight loss test was organized as follows: a

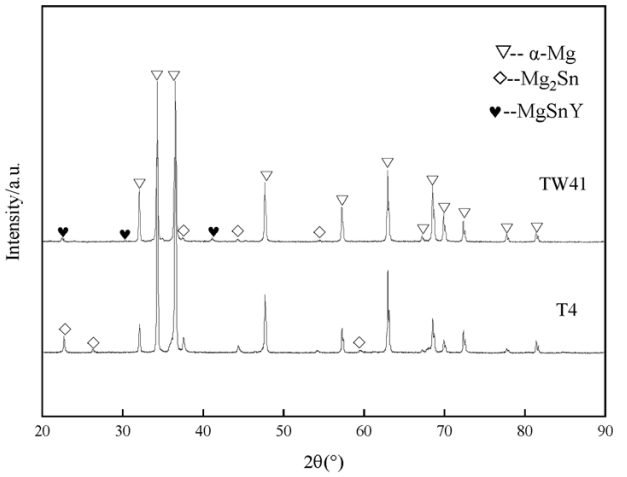

Figure 1: XRD patterns of the as-extruded T4 and TW41 alloys

(10 × 10 × 10) mm sample was immersed in the 3.5 *w*/% NaCl aqueous solution for 24 h, and the precipitated hydrogen was collected using a burette and recorded every 2 h. To maintain a stable concentration of the solution, the NaCl solution was replaced every 12 h, and after the corrosion was completed, the sample was removed and placed in the prepared chromate. It was washed under ultrasonic conditions for 10 min.

Equation (1) was used to calculate the loss-in-weight corrosion rate:[18]

$$P_{\mathrm{W}} = \frac{8.76 \cdot 10^4 \cdot \Delta g}{A \cdot t \cdot \rho} \tag{1}$$

Equation (2) was used to calculate the hydrogen evolution rate:[19]

$$P_{\mathrm{H}} = \frac{8.76 \cdot 10^4 \cdot \Delta V \cdot \mathrm{M}}{A \cdot t \cdot \rho} \tag{2}$$

where P_{W} – the loss-loss corrosion rate, mm year^{-1}; Δg – the mass loss before and after the alloy corrosion, g; ΔV – the total precipitation of hydrogen during corrosion, mL. The relationship between the rate of M-hydrogen production and the rate of alloy mass loss was 0.001083 g·mL^{-1}. A – The total surface area of the immersed sample, cm^2; t – the soaking time, h; ρ – the weight loss measurement specimen density, g·cm^{-3}.

3 RESULTS

3.1 Microstructure

XRD patterns of the as-extruded T4 and TW41 alloys are shown in **Figure 1**. It can be found that the as-extruded T4 alloy is mainly composed of two phases, a-Mg and Mg_2Sn; after adding 1 wt.% Y, in addition to α-Mg and Mg_2Sn, there is another phase in the alloy that cannot be identified with the XRD spectral database. Therefore, in order to further confirm the unknown phase, the composition of the unknown phase is obtained with scanning electron microscopy assisted X-ray spectroscopy (SEM-EDS), as shown in **Figure 2**. The elements of the D phase are composed of Mg, Sn and Y, and the atomic ratio of Sn and Y is close to 1:1, so it is speculated that the phase is MgSnY. Zhao et al.[20] also found that an addition of element Y to the Mg-1Sn alloys results in the formation of ternary phase MgSnY. In addition, it can be seen from **Figure 2** that the second phases of the two as-extruded alloys are streamlined along the extrusion direction (ED) on the matrix, and the volume fractions of the second phases of the alloy increase significantly after the addition of 1 *w*/% Y. The second phases of the as-extruded T4 alloy are Mg_2Sn (shown in **Figure 2a**) and Mg_2Sn, which are mainly bulk and granular. The second phases of the TW41 alloy are mainly Mg_2Sn and MgSnY (shown in **Figure 2b**), where Mg_2Sn is massive and granular, and MgSnY is of an irregular polygonal shape.

Figure 3 shows the distribution of IPF, PF and orientation angles of the as-extruded T4 and TW41 alloys. Both alloys exhibit a typical {0001} substrate ED extruded fiber texture. The maximum extreme density of T4 alloy substrate texture is 17.4, and the maximum extreme density of TW41 alloy substrate texture is 14.73. In addition, it can be seen that the proportion of

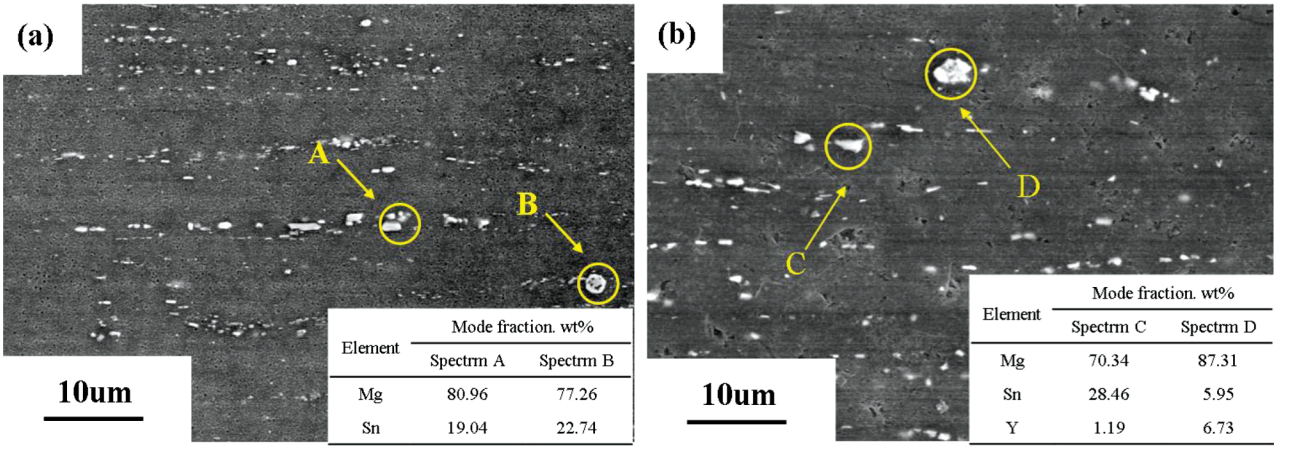

Element	Mode fraction. wt%	
	Spectrm A	Spectrm B
Mg	80.96	77.26
Sn	19.04	22.74

Element	Mode fraction. wt%	
	Spectrm C	Spectrm D
Mg	70.34	87.31
Sn	28.46	5.95
Y	1.19	6.73

Figure 2: Phase distribution of the as-extruded T4 and TW41 alloys

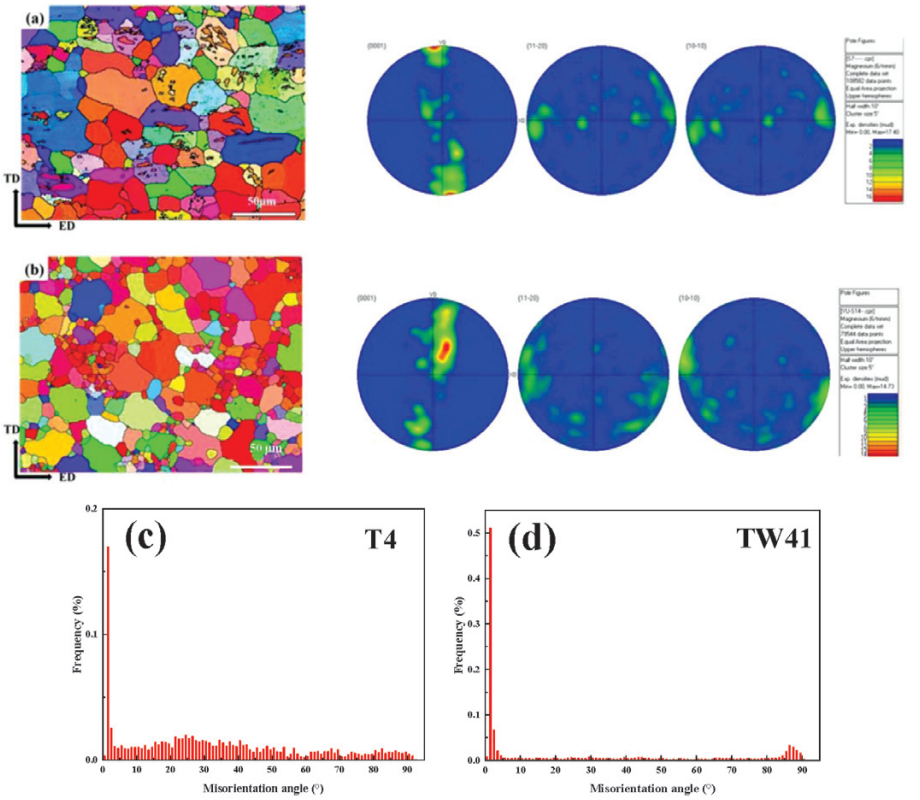

Figure 3: IPF and PF diagrams of extruded alloys: (a) T4, (b) TW41, (c)–(d) misorientation angle distribution of extruded alloys

small-angle grain boundaries of the two alloys is 9.38 % and 11.7 %, respectively, and the proportion of large-angle grain boundaries is 73.37 % and 36.55 %, respectively. The results show that the addition of Y can weaken the alloy basal weave strength and reduce the neighboring grain orientation difference. This is due to the fact that the MgSnY ternary phase precipitates after the addition of Y to the T4 alloy, and the precipitated phase particles produce particle-stimulated nucleation (PSN) during the hot extrusion process, resulting in a weak texture strength. It has been reported that coarse particles larger than 1 μm in size can trigger the particle stimulated nucleation (PSN) mechanism, which reduces the orientation correlation between the recrystallized grains and existing grains, thereby weakening the texture strength.[21]

Figure 4 shows dynamic recrystallization of the extruded T4 and TW41 alloys and the corresponding proportional distributions for each region. The blue, yellow, and red grains represent recrystallized, sub-crystalline, and deformed grains, respectively. It has been shown that complete dynamic recrystallization occurs when the extrusion temperature of magnesium alloys exceeds 350 °C.[22] It can be seen that the grains of the as-extruded T4 and TW41 alloys are equiaxed and partially recrystallized, indicating that the alloys underwent partial dynamic recrystallization after extrusion deformation at 300 °C. Between them, the proportion of dynamically recrystallized grains is 28 %, the proportion of sub-crystalline grains is 60 %, and the proportion of deformed grains is 12 %. Compared with the T4 alloy, the proportion of dynamically recrystallized grains increased significantly to 85 % after the addition of Y, while the proportion of sub-crystalline and deformed grains decreased to 12 % and 3 %, respectively. The results show that the addition of Y affects the dynamic recrystallization behavior of the alloy during the extrusion process, and can promote the dynamic recrystallization of T4 alloy. In addition, the average grain size of T4 alloy and TW41 alloy is 7.25 μm. The addition of Y can also refine the grain size of T4 alloy. It is concluded that the increase in the dynamic recrystallization fraction of the alloy is caused by the increase in the second phase particles of the alloy after the addition of 1 *w*/% Y (as shown in **Figure 2**), and the largest second phase particles can be accelerated by particle stimulation nucleation (PSN) due to a huge amount of energy stored in the deformation region. In addition, the grain refinement of the alloy is due to the fact that Y and Mg have the same close-packed hexagonal (hcp) crystal structure and similar lattice parameters, which conforms to the principle of "size and structure matching". Thus, Y can be used as a heterogeneous nucleation particle for α-Mg, making nucleation much easier. In addition, Y is the surfactant element of Mg, enriched at the solid-liquid interface during the solidification process of the alloy, resulting in a supercooling zone of the composition and thus inhibiting the growth of grains.

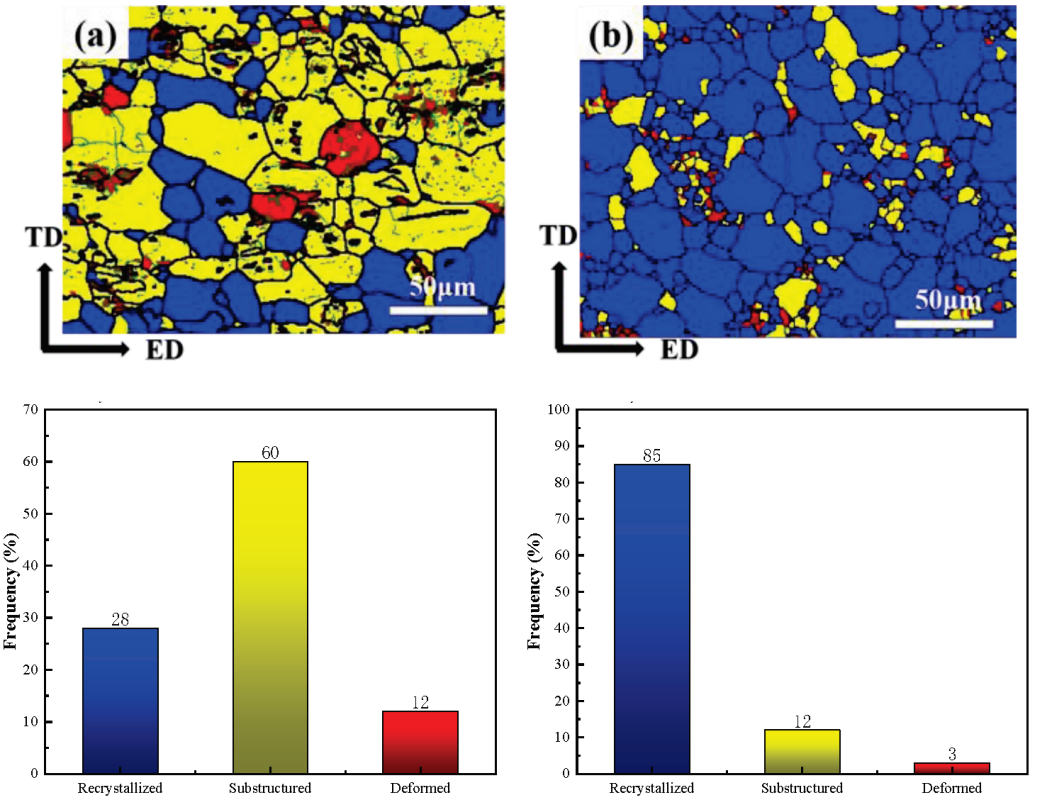

Figure 4: Dynamic recrystallization distribution map of as-extruded T4 and TW41 alloys: (a) T4, (b) TW41

3.2 Mechanical properties

The tensile mechanical properties of the as-extruded T4 and TW41 alloys at room temperature are shown in **Figure 5**, where it can be seen that Y has an effect on the yield strength (YS), ultimate tensile strength (UTS) and elongation of the alloys. The UTS of T4 and TW41 alloys was 219 MPa and 228 MPa; the YS was 135 MPa and 165 MPa, respectively, while the elongation was 14.7 % and 8.4 %, respectively. The results show that the as-extruded TW41 alloy had the highest UTS and YS, which were significantly higher than those of T4 alloy, but the elongation of TW41 alloy was reduced by 42 %. It is believed that the increase in the strength of TW41 alloy was due to the addition of Y, which refined the microstructure of the alloy, and the grain refinement led to the increase in the grain boundaries, making the transport of dislocations difficult, thereby improving the yield strength of the alloy. The reason for the decrease in the alloy elongation may have been due to the dislocation plugging caused by the largest second-phase particles precipitated in the alloy matrix, resulting in stress con-

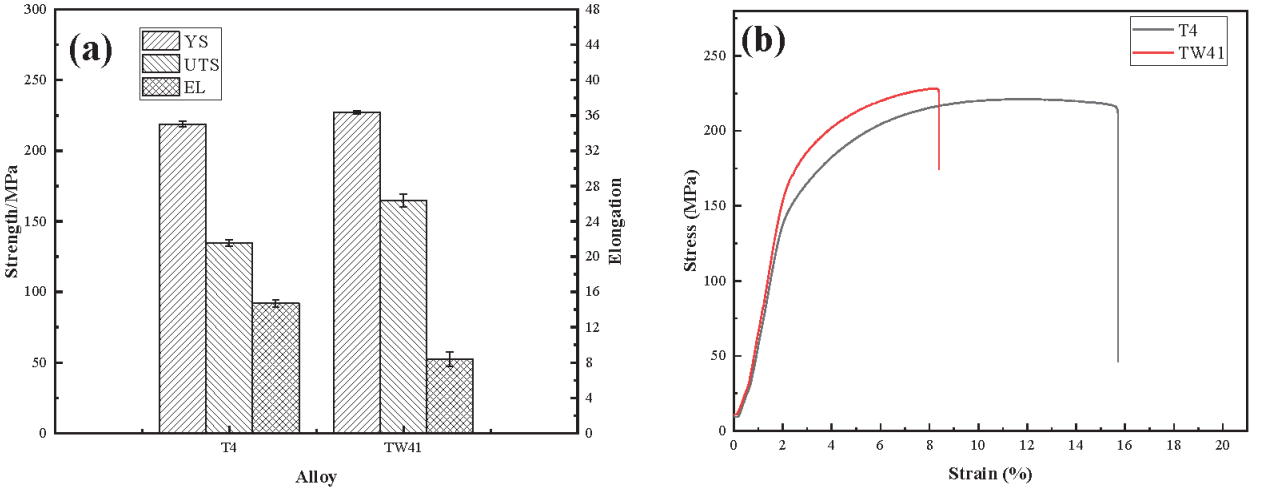

Figure 5: Mechanical properties of as-extruded alloys T4 and TW41

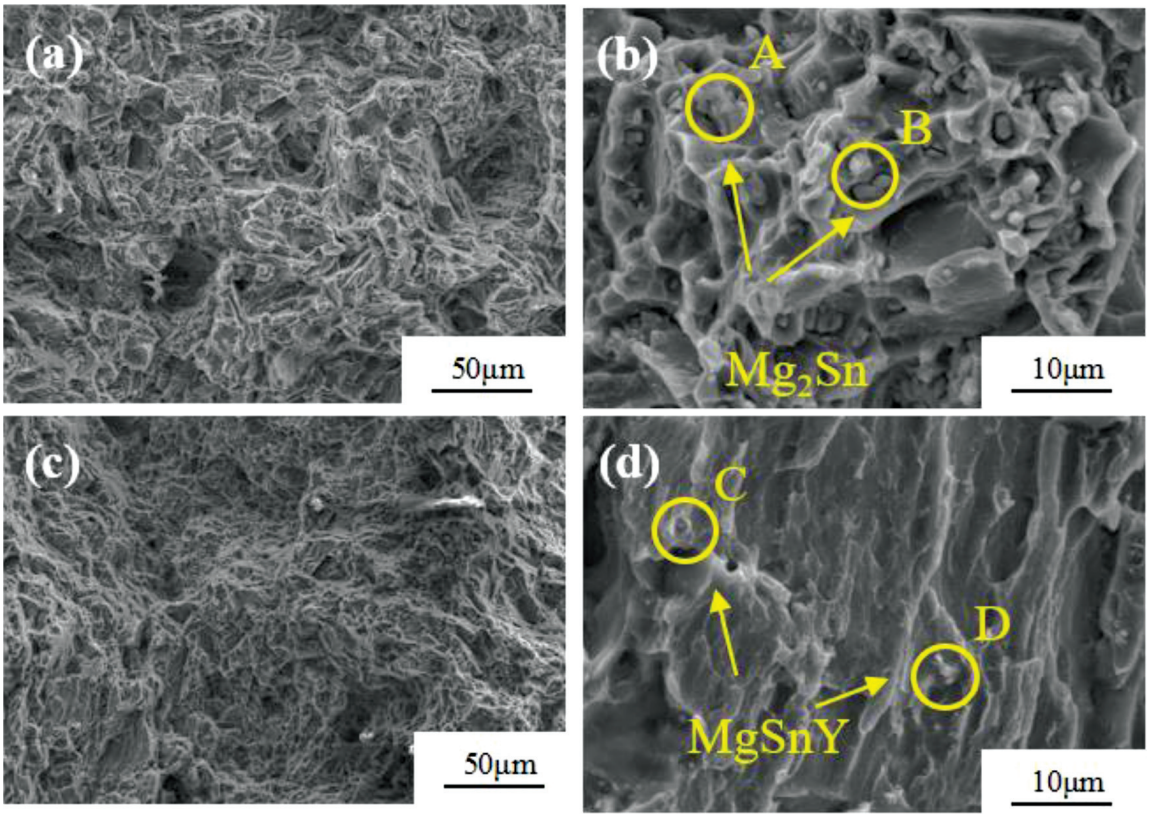

Figure 6: SEM fracture morphologies of the as-extruded alloy tensile fracture specimens : a)–b)T4, c)–d)TW41

centration and becoming the source of cracks, resulting in a significant decrease in the alloy elongation.

Figure 6 shows the room-temperature tensile fracture morphology of the extruded T4 and TW41 alloys. It can be seen that the fractures of T4 and TW41 alloys have dimples of different depths, showing ductile fracture characteristics. The size and depth of a dimple of the as-extruded T4 alloy are large and deep, and there is a massive Mg_2Sn phase (as shown with the EDS analysis in **Figure 7**) at the bottom of the dimple. On the contrary, compared with T4 alloy, the dimple size of TW41 alloy is shallow, and the second phase particles at the bottom of dimples are mainly the Mg_2Sn phase and MgSnY phase. Under tensile stress, stress concentration occurs at the interface between the Mg matrix and MgSnY phase particles, promoting the formation of cracks.

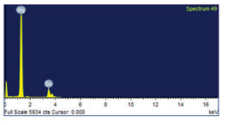

Element A	Weight%	Atomic%	
Mg K	68.93	91.55	
Sn L	31.07	8.45	
Totals	100.00		

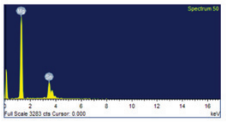

Element B	Weight%	Atomic%	
Mg	53.95	85.12	
Sn	46.05	14.88	
Totals	100.00		

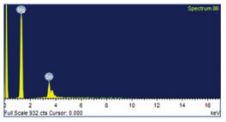

Element C	Weight%	Atomic%	
Mg	57.41	86.81	
Sn	42.59	13.19	
Totals	100.00		

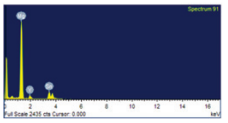

Element D	Weight%	Atomic%	
Mg	61.46	87.96	
Y	7.54	2.95	
Sn	30.99	9.09	
Totals	100.00		

Figure 7: EDS analysis of fracture phases in as-extruded T4 and TW41 alloys

3.3 Corrosion properties

The changes in the hydrogen volume and average corrosion rate of the two alloys after soaking for 24 h are shown in **Figure 8**. It can be seen that the hydrogen precipitation of the two alloys has a linear relationship with the immersion time, indicating that the amount of hydrogen produced in each time period is almost equal, while the amount of hydrogen precipitated by TW41 alloy is much higher than that of T4 alloy, indicating that its corrosion resistance is relatively poor.

Figure 9 shows the polarization curves and Nyquist plots of the as-extruded T4 and TW41 alloys. In general, the polarization curve reflects the corrosion thermodynamic tendency, and the impedance spectrum reflects the corrosion kinetic tendency. This is typically supplemented by EIS, reflecting the actual corrosion resistance of the material and the polarization curve.[23] As can be seen on **Figure 9a**, the corrosion potential of TW41 alloy is slightly higher than that of T4 alloy, indicating that

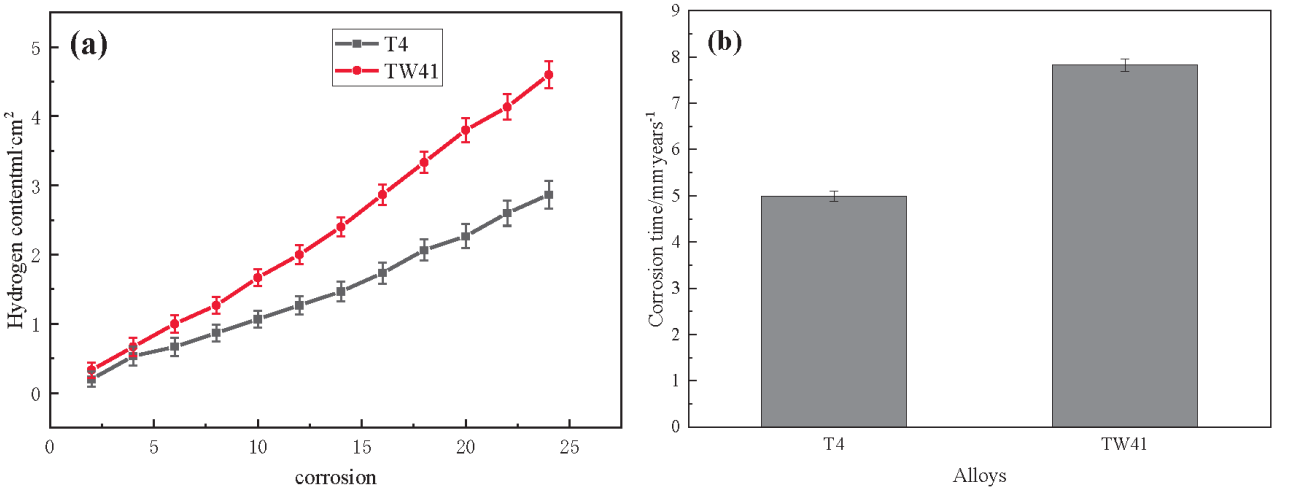

Figure 8: Corrosion of as-extruded T4 and TW41 alloys immersed for 24 h: (a) hydrogen content; (b) corrosion rate

the self-corrosion tendency of TW41 alloy is lower than that of T4 alloy from a thermodynamic point of view. In addition, the corrosion potential (Ecorr) and corrosion current density (Icorr) were fitted in combination with the polarization curves in **Table 1**. It can be seen that there is little difference between the two alloys in terms of corrosion potential; in terms of corrosion current density, TW41 alloy is slightly higher than T4 alloy, indicating that the corrosion resistance of TW41 alloy is poorer than that of T4 alloy. It is believed that the decrease in the corrosion tendency of the alloy may be caused by the precipitation of the MgSnY ternary phase due to Y element and the inhibition of the precipitation of Mg_2Sn phase, thereby reducing the galvanic corrosion tendency caused by the Mg_2Sn phase.

From the Nyquist curves in **Figure 9b**, it can be seen that there are a high-frequency capacitive arc and a low-frequency inductive arc resistance in the Nyquist curves of T4 and TW41 alloys, indicating that the addition of Y does not change the corrosion mechanism of T4 alloy. In addition, an inductive arc is present in the extruded T4 and TW41 alloys, indicating that pitting corrosion occurs during the corrosion process. Therefore, the impedance spectra of the as-extruded T4 and TW41 alloys are fitted to an equivalent circuit, shown in **Figure 9c**, and the specific parameters are shown in **Table 2**. Among them, Rs is the resistance of the solution, R_t is the resistance of the corrosion product film, R_L and L are connected in series to indicate pitting areas on the surface of the alloy, and the constant phase angle element

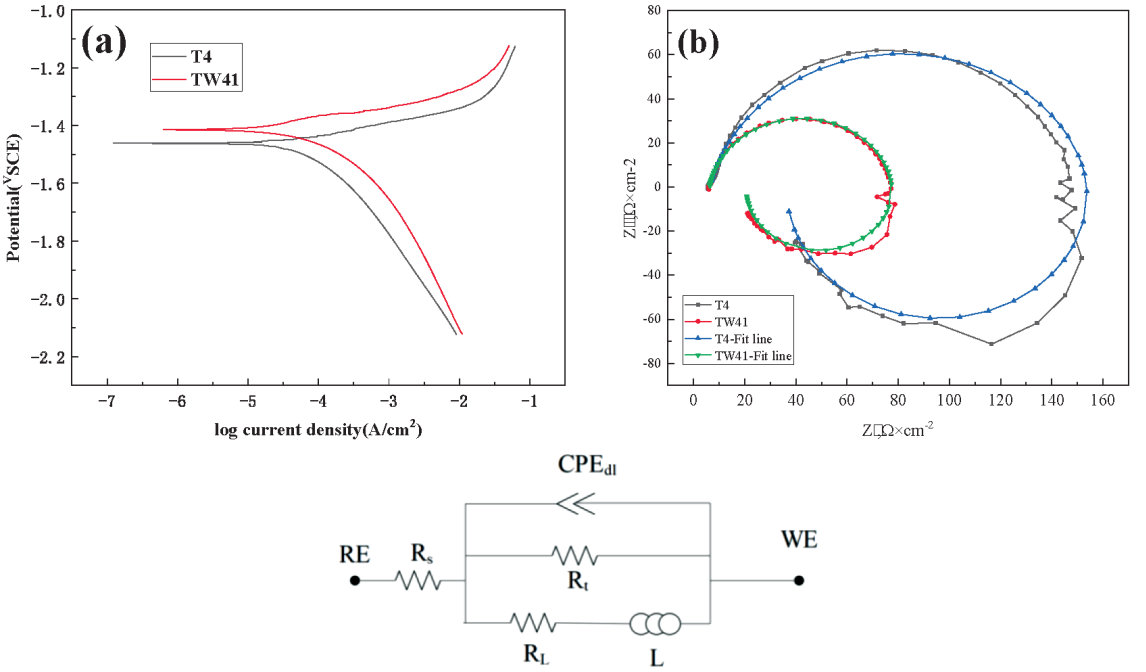

Figure 9: a) Polarization curves, b) Nyquist diagrams and fitting circuit of as-extruded T4 and TW41 alloys

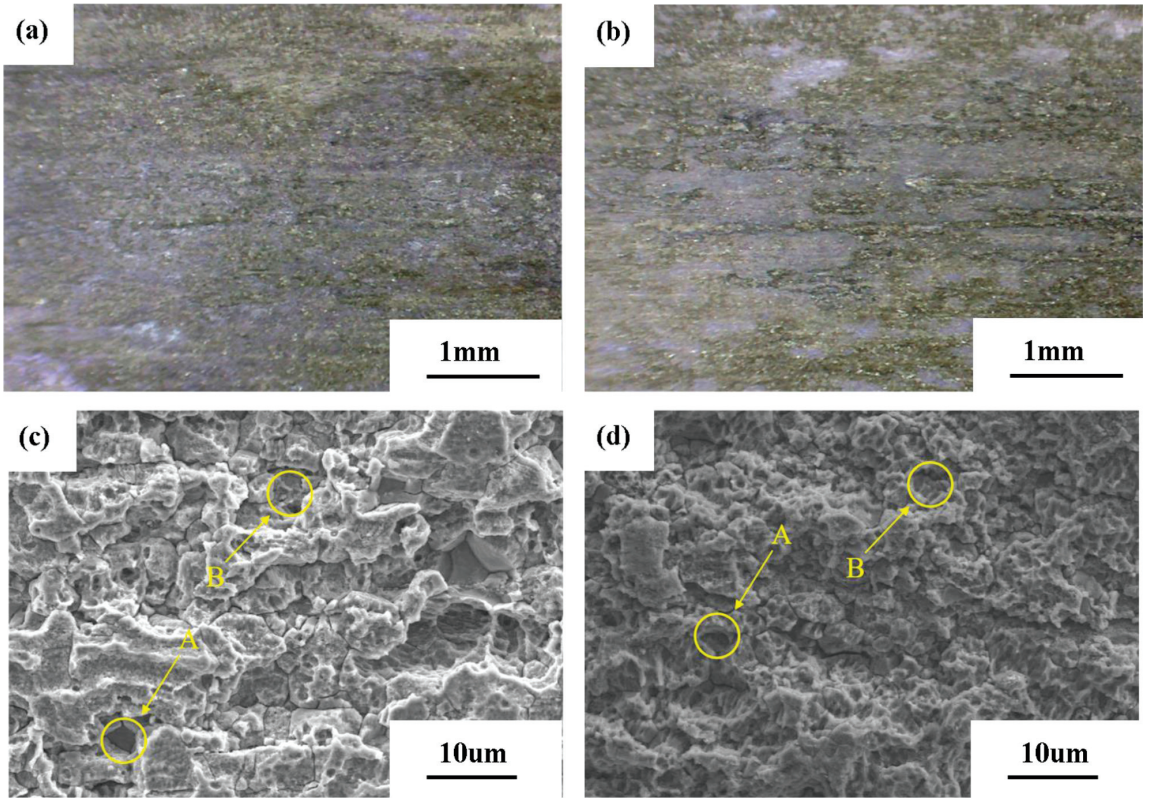

Figure 10: Macroscopic and SEM images of as-extruded T4 and TW41 alloys: (a), (c) T4; (b), (d) TW41

CPE_{dl} and resistor R_{ct} are connected in parallel to fit the high-frequency capacitive arc in the equivalent circuit. It is found that the charge transfer resistance R_t on the surface of T4 alloy is greater than that of TW41 alloy, indicating that the electrochemical corrosion rate of T4 alloy is relatively slow and the corrosion resistance is better.

Table 1: As-extruded T4 and TW41 alloys in 3.5 *w*/% NaCl

Alloy	E_{corr}/V	I_{corr}/ A·cm^2
T4	–1.461	1.5×10^{-5}
TW41	–1.414	2.5×10^{-5}

Table 2: Equivalent circuit fitting results of T4 and TW41 alloys

Alloy	R_s Ω·cm^2	CPE		R_t Ω·cm^2	R_L Ω·cm^2	L H·cm^2
		Y_1	n_1			
T4	6.102	8.90×10^{-5}	0.86	149.8	38.17	223
TW41	6.315	12.97×10^{-5}	0.90	71.93	17.63	104.5

Figure 10 shows macroscopic and SEM morphologies of the extruded T4 and TW41 alloys after 24 h of corrosion, with the corrosion products removed. Comparisons revealed that the as-extruded T4 alloy shows less surface corrosion than the TW41 alloy, and a metallic luster was observed on its surface. On the SEM images, we can see corrosion pits that occurred when the corrosion products were peeled off the surface of the as-extruded T4 and TW41 alloys. This is mainly due to the fact that the corrosion medium can penetrate the surface film and directly contact the Mg matrix after the occurrence of pitting, which causes the corrosion and dissolution of the α-Mg matrix, resulting in the second phase falling off and producing pits. In addition, it can be observed on **Figure 10** that the pits of TW41 alloy are deeper than those of T4 alloy, indicating that the corrosion resistance of T4 alloy is higher than that of TW41 alloy; it is believed that this is due to the addition of Y, which precipitates the ternary MgSnY phase and increases the volume fraction of the second phase. This increases galvanic corrosion between the second phase as the microcathode and the magnesium matrix, resulting in a rapid corrosion of the magnesium matrix around the second phase.

4 DISCUSSION

Studies have shown that the grain size, second phase, texture, or grain orientation of magnesium alloys are important factors affecting the properties of magnesium alloys.[24,25] The properties of an alloy are the results of a combination of factors such as grain size, second phase, microstructure uniformity, defect density, etc. In terms of mechanical properties, grain refinement leads to an increase in grain boundaries, making the transport of dislocations difficult, thereby increasing the strength of the alloy. In this study, the yield strength and tensile strength of the as-extruded alloy increased and the elongation decreased after the addition of Y to T4 alloy, which was mainly due to the effect of the addition of Y on the grain

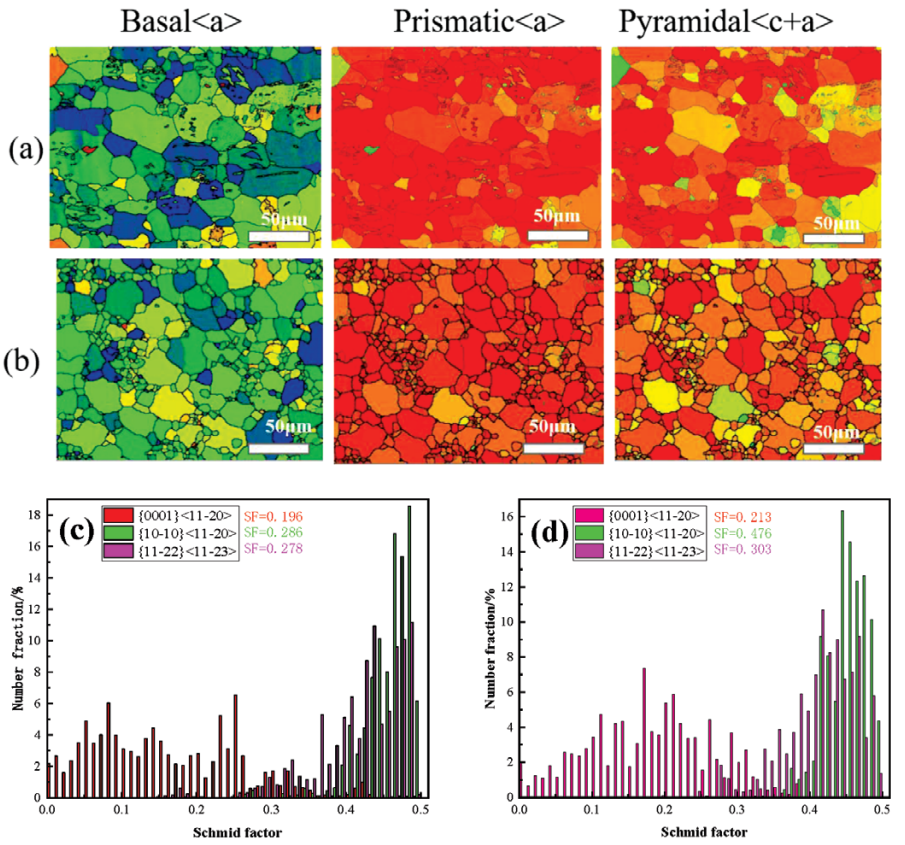

Figure 11: Distribution of Schmid factors: a), c) T4, b), d) TW41

refinement of the alloy and the effect of fine-grain strengthening. According to the Hall-Petch formula, the yield strength is inversely proportional to the grain size, and the yield strength of the alloy can be improved by fine grains, so the strength of TW41 alloy is increased.[26]

In order to further investigate the main deformation mechanisms of the two as-extruded alloys in this test, the Schmid factor diagram shown in **Figure 11** was determined. It was shown that the Schmid factor can qualitatively analyze the initiation of various dislocation slip mechanisms during plastic deformation of metals, and the initiation of a slip usually follows Schmid's law.[27] As can be seen on **Figure 11**, with the addition of 1 *w*/% Y, the basal, cylindrical and cone slip SF of the alloy increases significantly, resulting in an increase in the ductility of the alloy. In terms of corrosion performance, there is a similar Hall-Petch relationship between the corrosion current density and grain size of magnesium alloys. The grain boundary density increases due to the grain refinement, while the grain boundary, as a highly active region, increases the dissolution rate of the anode, thereby reducing the corrosion resistance of the alloy.[28] In this study, the corrosion resistance of the as-extruded TW41 alloy was better than that of the as-extruded T4 alloy, which was due to the increase in the grain boundary density caused by the addition of Y. The grain boundary, as a highly active region, accelerated the dissolution of the anode, thereby increasing the corrosion rate of TW41 alloy. In addition, the volume fraction of second phase of TW41 alloy is higher than that of T4 alloy, increasing the initiation sites for galvanic corrosion between the second phase and the magnesium matrix. This results in a rapid corrosion of the magnesium matrix around the second phase particles. Thus, the corrosion rate of TW41 alloy is higher than that of T4 alloy.

5 CONCLUSION

In this paper, the effects of a Y addition on the microstructure, mechanical properties and corrosion resistance of Mg-4Sn alloy are systematically studied, and the following conclusions are drawn:

- The addition of 1 wt.% Y element can refine the grain size of the extruded T4 alloy. The volume fraction of the second phase of TW41 alloy increases, and the precipitated second phase is mainly composed of the ternary MgSnY and the Mg_2Sn phases.
- The addition of 1 wt.% Y failed to change the texture type of the alloy, but it could weaken the texture strength of the alloy. The precipitated MgSnY phase in TW41 causes grain refinement in the alloy, leading to an increase in the grain boundaries. This increase makes dislocation motion more difficult, thereby improving the yield strength of the alloy.
- The addition of 1 *w*/% Y can increase the self-corrosion potential of T4 alloy, but an excessive second

phase increases the initiation sites for galvanic corrosion, thus increasing the corrosion current of the alloy and reducing the corrosion resistance.

Acknowledgements

The authors acknowledge the National College Students' Entrepreneurship Project (202311035033), the financial support from the Liaoning Province Natural Science Foundation Project of China (2023-MS-321) and the Liaoning Province International Cooperation Project (Project Number: 2023030491-JH2/107).

6 REFERENCES

[1] J. Song, J. Chen, X. Xiong, et al., Research advances of magnesium and magnesium alloys worldwide in 2021, J. Magnes. Alloy, 10 (**2022**), 863–898, doi:10.1016/j.jma.2022.04.001

[2] B. Jiang, G. Zhou, J. Dai, et al., Effect of second phases on microstructure and mechanical properties of as-cast Mg-Ca-Sn magnesium alloy, Rare Metal Mat. Eng., 43 (**2014**), 2445–2449

[3] F. Pan, B. Jiang, Development and application of plastic processing technology of magnesium alloy, Acta Metall. Sin., 57 (**2021**), 1362–1379, doi:10.11900/0412.1961.2021.00349

[4] Q. Yang, Y. Zeng, M. Zhou, et al., Effect of yttrium addition (0.2%) on the hot compression behavior of the as-cast Mg-Sn alloy, Rare Metal Mat. Eng., 48 (**2019**), 2275–2283

[5] H. Pan, C. Yang, Y. Yang, et al., Ultra-fine grain size and exceptionally high strength in dilute Mg–Ca alloys achieved by conventional one-step extrusion, Mater. Lett., 237 (**2019**), 65-68, doi:10.1016/j.matlet.2018.11.080

[6] Y. Zhang, X. Chen, Y. Lu, et al., Microstructure and mechanical properties of as-extruded Mg-Sn-Zn-Ca alloy with different extrusion ratios, T. Nonferr. Metal. Soc., 28 (**2018**), 2190–2198, doi:10.1016/S1003-6326(18)64864-2

[7] O. Sadeddin, M. Moazami, M. Nayyeri, Effect of hot extrusion on microstructure and mechanical properties of Mg-5Sn-xZr alloys, Met. Mater. Int., 27 (**2021**), 1996–5007, doi:10.1007/s12540-020-00919-y

[8] H. Zhou, X. Huang, L. Kong, et al., Research advances in corrosion behavior of magnesium alloy in marine atmospheric environment, Rare Metal Mat. Eng., 53 (**2024**), 1170–1180, doi:10.12442/j.issn.1002-185X.20230132

[9] Y. Chen, Ji. Zhou, Yong Liu, et al., Research progress on corrosion mechanism and regulation of magnesium alloy, Chinese Journal of Nonferrous Metals, 33 (**2023**), 3152–3170

[10] C. Gong, X. He, D. Fang, et al., Effect of second phases on discharge properties and corrosion behaviors of the Mg-Ca-Zn anodes for primary Mg-air batteries, J. Magnes. Alloy., 861 (**2021**), 158493, doi:10.1016/j.jallcom.2020.158493

[11] X. Xia, Y. Pan, X. Yuan, et al., Research progress of surface corrosion protection technology for Mg Alloys, Surface Technology, 52 (**2023**), 37–50+70, doi:10.16490/j.cnki.issn.1001-3660.2023.05.004

[12] L. Li, F. Li, J. Lei, et al., Research progress in effect of alloying elements on anti-corrosion performance of magnesium alloys, Materials Reports, 25 (**2011**), 110–113

[13] H. Ha, J Kang, C Yim, et al., Role of hydrogen evolution rate in determining the corrosion rate of extruded Mg–5Sn–(1–4 wt%) Zn alloys, Corros. Sci., 89 (**2014**), 275–285, doi:10.1016/j.corsci.2014.09.011

[14] C. Zhao. X. Chen, F. Pan, et al., Effect of Sn content on strain hardening behavior of as-extruded Mg-Sn alloys, Mat. Sci. Eng.: A, 713 (**2018**), 244–252, doi:10.1016/j.msea.2017.12.074

[15] X. Qian, Y. Zeng, B. Jiang, et al., Grain refinement mechanism and improved mechanical properties in Mg–Sn alloy with trace Y addition, J. Alloys Compd., 820 (**2020**), 153122, doi:10.1016/j.jallcom.2019.153122

[16] A. Issa, J. Saal, C. Wolverton, Physical factors controlling the observed high-strength precipitate morphology in Mg–rare earth alloys, Acta Mater., 65 (**2014**), 240–250, doi:10.1016/j.actamat.2013.10.066

[17] X. Yu, B. Jiang, H. Yang, et al., High temperature oxidation behavior of Mg-Y-Sn, Mg-Y, Mg-Sn alloys and its effect on corrosion property, Appl. Surf. Sci., 353 (**2015**), 1013–1022, doi:10.1016/j.apsusc.2015.07.011

[18] Z. Jia, B. Yu, Li. Fu, et al., Effect of Zn on corrosion resistance of extruded Mg-3Sn-1Ca alloy, Surface Technology, 52 (**2023**), 233–242, doi:10.16490/j.cnki.issn.1001-3660.2023.04.020

[19] C. Xiang, Z. Xiao, H. Ding, et al., Compressive properties and energy absorption characteristics of extruded Mg-Al-Ca-Mn alloy at various high strain rates, Materials, 14 (**2020**) 1, 87, doi:10.3390/ma14010087

[20] H. Zhao, G. Qin, Y. Ren, et al., Microstructure and tensile properties of as-extruded Mg-Sn-Y alloys, T. Nonferr. Metals Soc., 20 (**2010**), s493–s497, doi:10.1016/S1003-6326(10)60525-0

[21] H. Ånes, A. Helvoort, K. Marthinsen, Orientation dependent pinning of (sub) grains by dispersoids during recovery and recrystallization in an Al–Mn alloy, Acta Mater., 248 (**2023**), 118761, doi:10.1016/j.actamat.2023.118761

[22] Y. Meng, J. Yu, K. Liu, et al., The evolution of long-period stacking ordered phase and its effect on dynamic recrystallization in Mg-Gd-Y-Zn-Zr alloy processed by repetitive upsetting-extrusion, J. Alloys Compd., 828 (**2020**), 154454, doi:10.1016/j.jallcom.2020.154454

[23] J. Kwon, S. Baek, H. Jung, et al., Role of microalloyed Sm in enhancing the corrosion resistance of hot-rolled Mg-8Sn-1Al-1Zn alloy, Corros. Sci., 185 (**2021**), 109425, doi:10.1016/j.corsci.2021.109425

[24] W. Chen, J. Ma, C. Cui, et al. Texture role in the mechanical property improvement contributed by grain refinement for Mg-2.6 Nd-0.55 Zn-0.5 Zr alloy subjected to extrusion processŠJĆ. MAT SCI ENG: A, 831 (2022): 142185, doi:10.1016/j.msea.2021.142185

[25] G. Zhu, S. Wang, M. Zha, et al., Effect of rare earth element Ce on the bulk texture and mechanical anisotropy of as-extruded Mg-0.3Al-0.2Ca-0.5Mn alloy sheets, Acta Metall. Sin., 60 (**2024**), 1079–1090, doi:10.11900/0412.1961.2024.00044

[26] Y. Chai, B. Jiang, J. Song, et al., Improvement of mechanical properties and reduction of yield asymmetry of extruded Mg-Sn-Zn alloy through Ca addition, J. Alloys Compd., 782 (**2019**), 1076–1086, doi:10.1016/j.jallcom.2018.12.109

[27] Q. Wang, B. Jiang, A. Tang, et al., Ameliorating the mechanical properties of magnesium alloy: Role of texture, Mat. Sci. Eng.: A, 689 (**2017**), 395–403, doi:10.1016/j.jallcom.2018.12.109

[28] R. Zeng, K. Kainer, C Blawert, et al., Corrosion of an extruded magnesium alloy ZK60 component—The role of microstructural features, J. Alloys Compd., 509 (**2011**) 13, 4462–4469, doi:10.1016/j.jallcom.2011.01.116